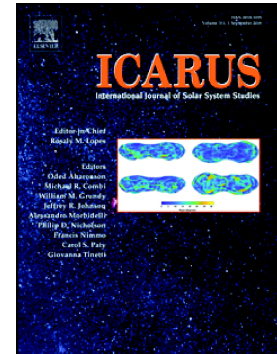


## Journal Pre-proof

Elemental composition, mineralogy and orbital parameters of the Porangaba meteorite

Martin Ferus, Lukáš Petera, Jakub Koukal, Libor Lenža, Barbora Drtinová, Jakub Haloda, Dalibor Matýsek, Adam Pastorek, Vojtěch Laitl, Renato Cassio Poltronieri, Marcelo Wagner Domingues, Gabriel Gonçalves, Rodrigo del Olmo Sato, Antonín Knížek, Petr Kubelík, Anna Křivková, Jiří Srba, Carlos Augusto di Pietro, Milan Bouša, Tomáš Vaculovič, Svatopluk Civiš



PII: S0019-1035(18)30587-6

DOI: <https://doi.org/10.1016/j.icarus.2020.113670>

Reference: YICAR 113670

To appear in: *Icarus*

Received date: 5 September 2018

Revised date: 17 January 2020

Accepted date: 27 January 2020

Please cite this article as: M. Ferus, L. Petera, J. Koukal, et al., Elemental composition, mineralogy and orbital parameters of the Porangaba meteorite, *Icarus*(2020), <https://doi.org/10.1016/j.icarus.2020.113670>

This is a PDF file of an article that has undergone enhancements after acceptance, such as the addition of a cover page and metadata, and formatting for readability, but it is not yet the definitive version of record. This version will undergo additional copyediting, typesetting and review before it is published in its final form, but we are providing this version to give early visibility of the article. Please note that, during the production process, errors may be discovered which could affect the content, and all legal disclaimers that apply to the journal pertain.

# Elemental Composition, Mineralogy and Orbital Parameters of the Porangaba Meteorite

Martin Ferus,<sup>1,†</sup> Lukáš Petera,<sup>1,2†</sup> Jakub Koukal,<sup>1,3,†</sup> Libor Lenža,<sup>1,3,†</sup> Barbora Drtinová,<sup>4</sup> Jakub Haloda,<sup>5,6</sup> Dalibor Matýsek,<sup>7</sup> Adam Pastorek,<sup>1,4</sup> Vojtěch Laitl,<sup>1</sup> Renato Cassio Poltronieri,<sup>9</sup> Marcelo Wagner Domingues,<sup>8</sup> Gabriel Gonçalves,<sup>8</sup> Rodrigo del Olmo Sato,<sup>9</sup> Antonín Knížek,<sup>1,12</sup> Petr Kubelík,<sup>1,10</sup> Anna Křivková,<sup>1,4</sup> Jiří Srba,<sup>3</sup> Carlos Augusto di Pietro,<sup>8</sup> Milan Bouša,<sup>1</sup> Tomáš Vaculovič,<sup>11</sup> Svatopluk Civiš,<sup>1,\*</sup>

<sup>†</sup> Contribution of all the first four authors is equal

- <sup>1</sup> **J. Heyrovský Institute of Physical Chemistry, Czech Academy of Sciences**  
Dolejškova 3, CZ18223 Prague 8, Czech Republic.
- <sup>2</sup> **Charles University in Prague, Faculty of Science**  
Hlavova 2030/8, CZ12843 Prague 2, Czech Republic.
- <sup>3</sup> **Valašské Meziříčí Observatory**  
Vsetínská 78, CZ75701 Valašské Meziříčí, Czech Republic.
- <sup>4</sup> **Faculty of Nuclear Sciences and Physical Engineering, Czech Technical University in Prague**  
Břehová 78/7, 115 19 Prague 1, Czech Republic.
- <sup>5</sup> **Czech Geological Survey**  
Klárov 131/3, CZ 118 21 Prague 1, Czech Republic.
- <sup>6</sup> **Oxford Instruments Nanotechnology Tools Ltd.**  
Velvarská 1649/13, CZ16000, Prague 6, Czech Republic
- <sup>7</sup> **VŠB-Technical University of Ostrava, Department of Geological Engineering**  
17. listopadu 15/2172, CZ708 33 Ostrava - Poruba, Czech Republic
- <sup>8</sup> **BRAMON**  
BRAZilian Meteor Observation Network
- <sup>9</sup> **Sociedade Brasileira de Meteorítica**  
R. Felipe Schmidt 735, Andar 4 Apt 401, Centro, Florianopolis, SC, CEP 88010-002, Brasil.
- <sup>10</sup> **Institute of Physics, Czech Academy of Sciences, Department of Radiation and Chemical Physics**, Na Slovance 2, CZ18221 Prague 8, Czech Republic
- <sup>11</sup> **Masaryk University, Faculty of Science, Department of Chemistry**, Kamenice 5, 62500 Brno
- <sup>12</sup> **Charles University in Prague, Faculty of Science, Department of Physical and Macromolecular Chemistry**  
Hlavova 2030/8, CZ12843 Prague 2, Czech Republic.

Corresponding author: Prof. Svatopluk Civiš (svatopluk.civis@jh-inst.cas.cz)

**Keywords: LIBS, EDS, Porangaba**

**Content:**

Abstract .....	3
1.2 History of Porangaba fall .....	5
2. Materials and Methods .....	8
2.1. Instrumentation.....	8
2.1.1. Electron microscopy and microanalysis .....	10
2.1.2. LIBS.....	11
2.1.3. ICP-MS and LA ICP-MS.....	11
2.1.4. AAS .....	12
2.2. Calculation of the trajectory .....	13
3. Results .....	14
3.1. Petrography and mineral composition.....	14
3.2. Bulk elemental composition.....	21
3.3. Trajectory and probable origin of the meteoroid.....	23
3.4. Simulation of Porangaba meteor spectra.....	25
4. Discussion .....	28
5. Conclusions .....	31
Acknowledgements .....	31
References .....	32

**Abstract**

The main objective of this study is to provide data on the bulk elemental composition, mineralogy and the possible origin of the Porangaba meteorite, whose fall was observed at 17:35 UT on 9 January 2015 on several sites of the state of São Paulo in Brazil. The surface of the meteorite was mapped by Scanning Electron Microscopy (SEM) and optical microscopy. The mineralogy and the bulk elemental composition of the meteorite were studied using Energy-Dispersive and Wavelength-Dispersive X-ray Spectroscopy (EDS/WDS) together with Electron BackScatter Diffraction (EBSD). The bulk elemental composition was also independently analysed by Atomic Absorption Spectrometry (AAS), Inductively Coupled Plasma Mass Spectrometry (ICP-MS), Laser Ablation ICP MS (LA ICP-MS) and Calibration-Free Laser-Induced Breakdown Spectroscopy (CF-LIBS). Based on the available visual camera records of the Porangaba meteorite fall, its orbit was tentatively calculated, and possible candidates for the source bodies in the Solar system were proposed. We also present a laboratory simulation of a Porangaba-like (L4 Ordinary Chondrite) meteor emission spectra. These can be used as benchmark spectra for the identification of meteor rock types through their comparison with meteor spectra recorded by high-speed video-cameras equipped with simple grating spectrographs.

## 1. Introduction

Complex analyses of meteors and meteorites play a key role in understanding the geology and history of rocky bodies, such as asteroids, comets, planets and moons, in the Solar system and beyond (Afanasiev et al., 2007)(Siraj and Loeb, 2019). Physical and chemical characterization of meteorites and meteors together with the knowledge of their trajectories or their origin in the Solar system provides information about the formation and subsequent evolution of the source body and ultimately about the history of Solar system itself.

The most detailed and reliable data are obtained by direct analysis of the chemical composition, mineralogy and petrology of meteorites. These data are especially valuable if the meteoroid trajectory during descent is recorded as well, because then, the meteoroid's source region can be determined. This is actually one of the major goals of current planetary science research (Drouard et al., 2018). However, as much as 80 % of the observed meteoroid falls are not paired with a corresponding meteorite found on Earth (Drouard et al., 2018). There are over 1000 known cases of observed falls, but the precise orbital trajectory has been calculated only for about 30 of them (Gounelle et al., 2006), ("List of meteorites with a complete 'lineage,'" 2019). The first meteorite with known orbital parameters and mineralogy was meteorite Příbram (7 April 1959, near Příbram, Czech Republic (Ceplecha, 1961)). Other known cases are for instance the Košice meteorite, Slovakia (Ozdin et al., 2015), (Horňáčková et al., 2014), the famous reconstruction of the Orgueil meteorite trajectory from historical records (Gounelle et al., 2006), the Lost City meteorite in Oklahoma, USA (McCrosky et al., 1971)(Gritsevich, 2008), Innisfree in Canada, Neuschwanstein in Germany, Peekskill in New York state, USA (Brown et al., 1994), Morávka in Czech Republic (Borovička et al., 2003), Park Forest in Illinois, USA, (Brown et al., 2004) and Chelyabinsk in Russia (Borovička et al., 2013).

The limiting factors of the survival of meteoroids during their descent to the Earth's surface can be calculated (see e.g. (Collins et al., 2005)). Given the nature of bodies entering the atmosphere, most meteoroids do not survive and it is therefore impossible to study their samples in laboratory. A potentially applicable method of overcoming this problem is classification based on the spectroscopy of ablation plasma formed around the meteoroid body by collisions with air molecules during its fall. This ablation melts the meteoroid surface, evaporates the body and forms a high temperature shock region in front of the meteoroid body. Emission spectra of the meteoroid plasma store basic information about their elemental composition. Such knowledge allows the classification of the object. Together with

descent geometry, spectroscopy enables the recalculation of the meteoroid atmospheric path, its orbit and eventually the determination of its source region in the Solar system. However, the reliability of this method is still subject to discussion (Drouard et al., 2018), (Ferus et al., 2018), (Ferus et al., 2017) (Koukal et al., 2016), (Jenniskens, 2007), (Borovicka, 1993), (Madiedo et al., 2013).

Classical study of real meteorite samples, therefore, remains the only established method and publications focused on detailed analysis of rare specimens of meteorites with known atmospheric paths are highly important. In our study, we explore the bulk elemental composition, mineralogy and the possible source of the famous Porangaba meteorite. The mineralogy and the bulk elemental composition of the meteorite was studied and a surface mineral map was obtained using Energy-Dispersive and Wavelength-Dispersive X-ray Spectroscopy (EDS/WDS) together with Electron Backscatter Diffraction (EBSD). The bulk elemental composition was independently determined by Atomic Absorption Spectrometry (AAS), Inductively Coupled Plasma Mass Spectrometry (ICP-MS), Laser Ablation ICP MS (LA ICP-MS) and Calibration-Free Laser-Induced Breakdown Spectroscopy (CF-LIBS). Based on visual camera records of the Porangaba meteorite fall and using UFOOrbit software (SonotaCo, 2009), its orbit was tentatively calculated and possible candidates of source bodies in the Solar system are proposed here. Simulation of the Porangaba-like (L4 ordinary chondrite) meteor is also provided. This should serve for classification purposes by comparison with records by high-speed video-cameras equipped with simple grating spectrographs.

## 1.2 History of Porangaba fall

Porangaba (Grossman, 2015) was a very bright daytime bolide that was observed at approximately 17:35 UT on 9 January 2015, in many areas of the state of São Paulo in Brazil. Carlos Augusto di Pietro (BRAZilian Meteor Observation Network, hereafter BRAMON) and Rodrigo del Olmo Sato (Sociedade Brasileira de Meteorítica) calculated the trajectory and the possible rubble field based on two photos of the dust trails from the cities of Lençóis Paulista (Figure 1, panel A), and Tatuí (Figure 1, panel B), as well as from video recording from a security camera (Lençóis Paulista). The first piece of this meteorite was found on the same day at S23.159° W48.181°, 6.4 km west-northwest of Porangaba, São Paulo, Brazil. The meteorite had a diameter of 8 cm and weighed 450 g (Figure 1, Panel C and D, detail in Panel E).

Using these calculations, the second meteorite was found by Julio Carvalho da Silva buried in a small impact crater, which was approximately 10 cm wide and 25 cm deep. Renato Cassio Poltronieri (BRAMON) and M.E. Zucolotto explored the calculated impact area on 18 January. The field location was actually very close to the area calculated by C.A. di Pietro and R. del Olmo Sato. A small fragment was removed and was studied at Museu Nacional in Rio de Janeiro (Grossman, 2015).

A second meteorite search expedition was undertaken between 30 January and 1 February. The expedition was organised by a group of BRAMON members. They found a third, heavier meteorite weighing 520 g on 10 January 2015 (Figure 1, Panel F). This meteorite was cut into five parts. Subsequently, a specimen of this meteorite weighing 26.7 g was sent to Czechia for analysis. In the current study, we report the results of the analysis of this specimen based on a combination of several different techniques.

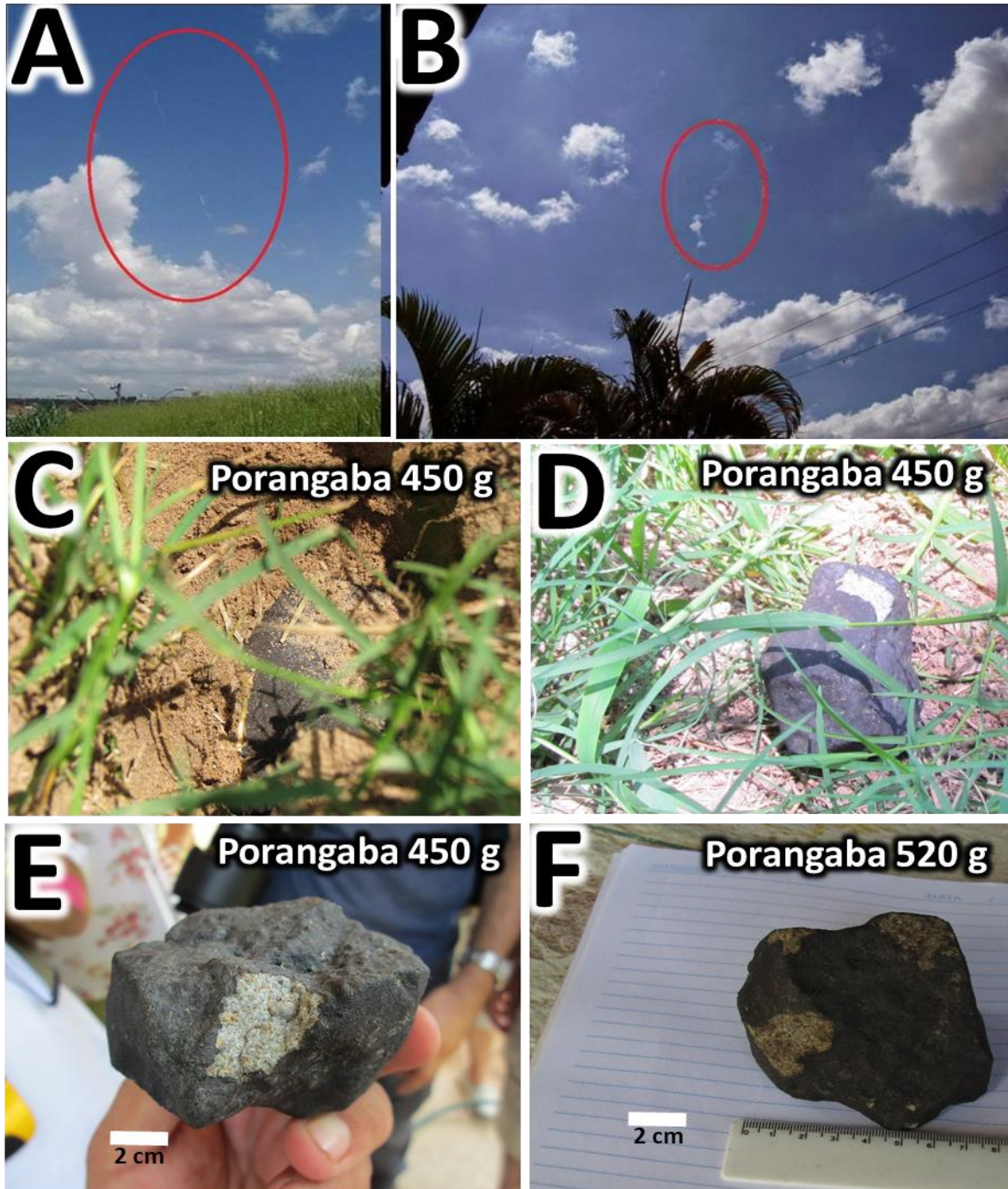


**Figure 1.** Panel A shows a photograph of the persistent trail of the Porangaba bolide as photographed from the city of Lençóis Paulista. The persistent trail of the Porangaba bolide as photographed from the city of Tatuí is shown in the panel B. Two large pieces, 450 g and 520 g, discovered close together in impact area, are depicted in the panels C – F.

## 2. Materials and Methods

### 2.1. Instrumentation

The 26.7 g Porangaba meteorite specimen was cut in two pieces (Figure 2). The part denoted as A (Panel A1-A2, Figure 2) was selected for mineralogical study, which was done at the Czech Geological Survey. The surface of the meteorite was mapped and photographed by Scanning Electron Microscopy (SEM) and optical microscopy. The mineralogy and the bulk elemental composition of the meteorite were determined by EDS/WDS together with EBSD. While EDS is faster, it is less accurate. WDS is slower but provides higher resolution and thus accuracy. In this case, WDS was used mainly for analysis of trace elements. EBSD was used for the determination of different mineral phases in the studied sample. All four techniques mentioned above (SEM, EDS/WDS and EBSD) ultimately provide a mineral phase distribution map of part of the studied meteorite specimen (Figure 5).

Part B (Panel B1-B2, Figure 2) of the Porangaba sample was studied by a variety of techniques. Due to the high sample heterogeneity, several techniques were combined to obtain more accurate results, namely AAS, ICP-MS, LA ICP-MS and CF-LIBS. The CF-LIBS study was performed at the department of spectroscopy at the J. Heyrovský Institute of Physical Chemistry. CF-LIBS with optical detection of the emitted laser induced plasma (Ciucci et al., 1999), (Tognoni et al., 2010) is limited to local analysis. This method does not represent a standard technique for the exploration of meteorite composition. However, it has been already employed in several studies (Cousin et al., 2012; De Giacomo, 2011; Dell'Aglio et al., 2014, 2010; Ferus et al., 2018; Hornackova et al., 2014; Lasue et al., 2012; Ozdin et al., 2015; Senesi, 2014; Thompson et al., 2006). Local microanalysis of major, minor and trace elements in the meteorite sample was performed by LA-ICP-MS on the same specimen, which was done at the Department of Chemistry at the Faculty of Science at the Masaryk University.

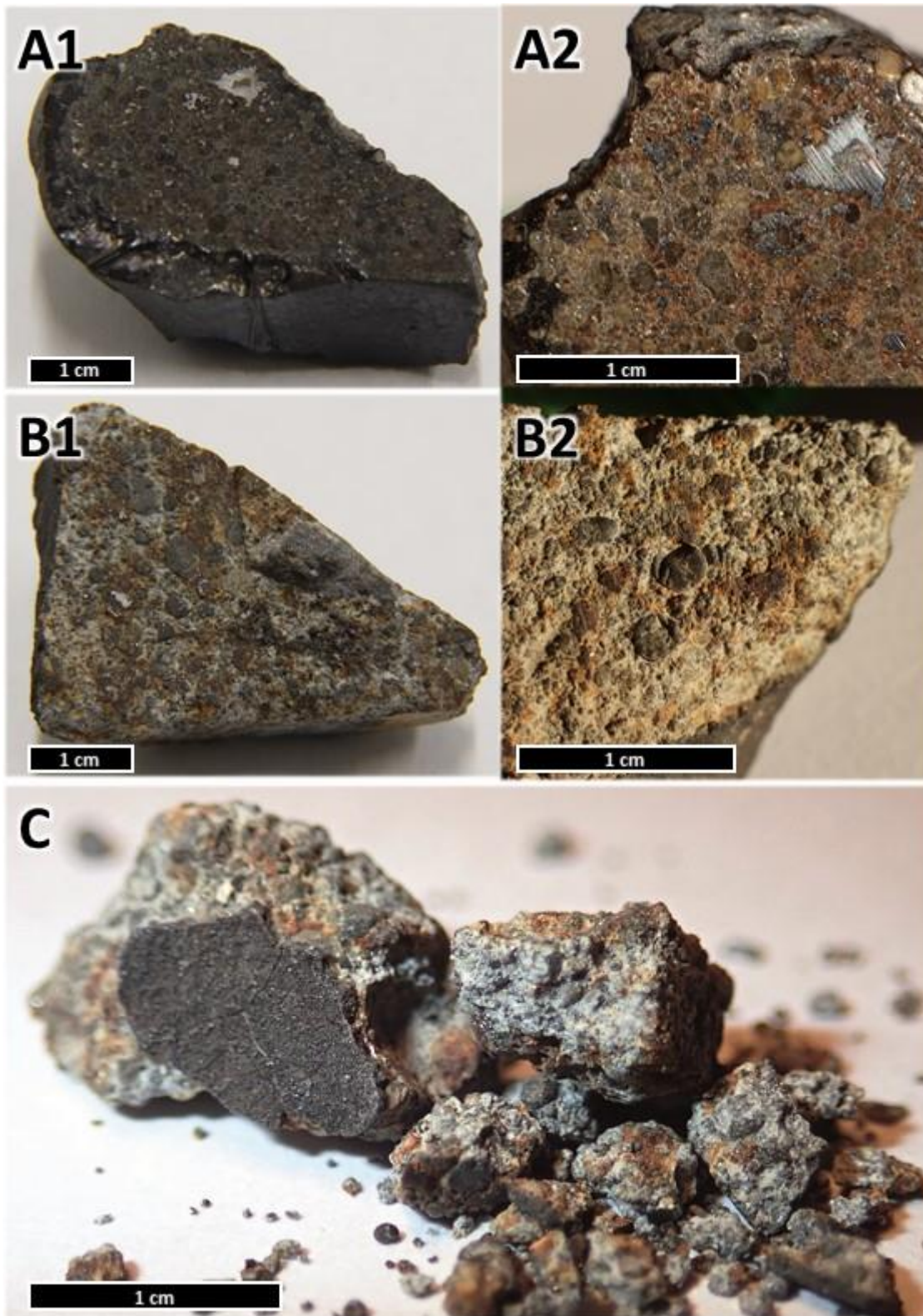


**Figure 2.** Photography of our specimen of Porangaba meteorite used for analysis in this study. Panel A1 shows part A of our specimen, which was used for the SEM, EDS/WDS and EBSD analysis. Panel A2 shows a more detailed view of part A. Panel B1 shows part B of our specimen, which was used for CF-LIBS and LA-ICP-MS analysis and panel B2 shows a more detailed view of part B. Panel C shows crushed part B, which was used for ICP-MS and AAS analysis.

Finally, this specimen was partially crushed (Panel C, Figure 2) and used for ICP-MS and AAS analyses. The ICP-MS was performed in the same laboratory on a 0.5 g of decomposed sample. The AAS was conducted at the Department of Nuclear Chemistry at the Faculty of Nuclear Sciences and Physical Engineering, Czech Technical University in Prague.

### **2.1.1. Electron microscopy and microanalysis**

Part A of the Porangaba sample (Panel A1 – A2, Figure 2.) was polished and subsequently coated with a 30-nm-thick conductive layer of carbon.

A TESCAN MIRA 3GMU (Czech Geological Survey in Prague, Czech Republic) SEM, was used for all the microanalytical studies and for the collection of backscattered electron images and elemental distribution maps. The mineral composition was determined with an Oxford Instruments AZtec Energy Automated analytical system with an X-ray energy dispersive spectrometer equipped with a Silicon drift detector (SDD) X-Max<sup>N</sup> 80 Premium (EDS) and an X-ray wavelength dispersive detector Wave 700 (WDS). Both analytical systems installed on the SEM were used for simultaneous EDS/WDS analyses. The analyses were performed at an accelerating voltage of 15 kV, a 20 nA beam current, a 0.090  $\mu\text{m}$  beam size and XPP matrix correction procedures. The acquisition of live measurements for the analysis of the major elements using EDS occurred every 60 s with an output count rate 110 kcps. The time steps for the measurements of the minor and trace elements using the WDS system were 20 or 30 s. To avoid Na and K ion migration during the analysis of glass and feldspar, the beam diameter was increased to 5  $\mu\text{m}$ . For the simultaneous EDS/WDS analysis, a combination of natural and synthetic standards was used for the standardisation and calibration procedures.

SEM images and elemental EDS/WDS distribution maps were generated with an accelerating voltage of 15 kV and a 2 - 10 nA range of the beam current. AZtec Energy Automated software was used to collect multiple wide-range elemental distribution maps covering several randomly selected areas of the meteorite surface. Each elemental distribution map was collected with a resolution of  $512 \times 512$  pixels with a pixel size of 1  $\mu\text{m}$ , where each pixel represents a measurement point from the X-ray spectrum. All the collected X-ray elemental distribution maps were processed using dedicated analytical procedures (TrueMap and Pulse Pile-Up Correction) implemented within the AZtec Energy software to solve the peak overlaps using deconvolution and background subtraction. Sets of elemental distribution maps covering entire regions of the studied section were merged into one dataset for future processing. The subsequent processing of the elemental distribution datasets allows us to study the mineral and chemical characteristics of the samples across the whole thick section

on a microscale. The mineral modes and average chemical compositions of the minerals that were present were determined using this dataset and the AZtec PhaseMap software module.

The integrated EBSD was performed by Oxford Instruments AZtec HKL Automated and Nordlys Nano detector, which was installed on the scanning electron microscope mentioned above and was used to confirm the microstructural characteristics of the studied minerals. The analytical parameters used included a 15 mm working distance, 20 kV accelerating voltage and 3.5 nA beam current.

### **2.1.2. LIBS**

The specimen B of sample of the Porangaba meteorite was taken and, without any additional preparation, irradiated by a 10 Hz pulsed nanosecond ArF laser ( $\lambda = 193$  nm, with a laser pulse width of 12 ns, frequency of 10 Hz, 1 mm<sup>2</sup> laser ablation spot and output energy of 180 mJ) in an ambient atmosphere. Before each measurement, the surface spot was cleaned by 5 laser pulses. The emission signal from the plasma was collimated and analysed using Echelle high resolution spectrograph (ESA 4000, LLA Instruments GmbH, Germany). The spectrograph allows for the simultaneous measurements of complex spectra in the range 200 – 780 nm, with an effective resolution ranging from 0.005 nm (at 200 nm) to 0.019 nm (at 780 nm). All the atomic spectra recorded by Echelle spectrograph were calibrated against mercury lines. In our measurements, the spectrograph was set to trigger a 12 ns laser pulse, a measurement delay of 4  $\mu$ s was used, and the gate was opened for 5  $\mu$ s for a total accumulation of 30 LIBS spectra. The low-resolution spectrum was simultaneously recorded by QHI astronomical camera equipped with 1/1000 mm holographic grating. The resulting resolution of the image was 0.4 nm/px. Elemental composition was calculated by CF method, as described in detail the Supplementary Data to the paper.

### **2.1.3. ICP-MS and LA ICP-MS**

Local microanalysis of major, minor and trace elements in the meteorite sample was performed by LA-ICP-MS. Laser ablation was performed at 35 points. The setup consists of laser ablation system LSX-213 G+ (Teledyne, USA) and quadrupole ICP-MS Agilent 7900 (Agilent Technologies, Japan). The ablation system is equipped with a Nd:YAG laser emitting radiation with the wavelength of 213 nm. The sample is placed in an ablation cell (Supercell®, New Wave, USA) where the interaction of the laser radiation with the sample occurs. The ablated material is transported by a carrier gas (helium) with a flow rate 1.0 l/min

into ICP-MS. The sample gas (argon) with flow rate 0.6 l/min is admixed to the carrier gas flow behind the ablation cell.

The determination of the overall elemental content in the meteorite sample was done by ICP-MS (Agilent 7900). A 0.5 g was leached in 5 ml of aqua regia and then transferred to 50 ml of deionized water. The leaching was done in triplicates. Before the ICP-MS analysis, the sample was diluted by factor of a 100.

ICP-MS parameters (gas flow rates, sampling depth, electrostatic lenses' voltages of the MS) were optimized in respect to maximize the S/N ratio and counts ratio of ThO<sup>+</sup>/Th<sup>+</sup> and U<sup>+</sup>/Th<sup>+</sup> lower than 0.2 and 1.1 %, respectively. All LA-ICP-MS measurements were done in a single hole drilling mode with laser spot diameter of 100 µm, laser fluence of 7,5 J/cm<sup>2</sup> and repetition rate 10 Hz. For quantification purposes, the certified reference material NIST 610 was used. All measurements were normalized to the total oxide content.

#### **2.1.4. AAS**

The contents of Fe, Ni, Co, Mg, Al, Na, Ca, K, Mn, Cr and Ti in part B (Figure 2, Panel C) were determined by AAS.

After crushing 9 g of the solid sample in an agate mortar, a magnetic (2.47 g) and a non-magnetic fractions (6.25 g) (Haramura et al., 1983; Van Der Auwera et al., 1998; Welten et al., 2011) were separated by a filter paper coated magnet. Both fractions were acid dissolved using distilled, ultra-pure reagents. Throughout the whole procedure, all weights were corrected for moisture content by drying the solid to constant weight at 105 °C.

The magnetic fraction was purified from silicates using HCl and concentrated HF treatment (Welten et al., 2011), while the weight of the sample was reduced from 0.7 g to 0.25 g. An aliquot weighing 0.1 g was then dissolved in 1:2 HNO<sub>3</sub>/HCl and slowly evaporated. The residue was dissolved in HNO<sub>3</sub> and transferred to demineralized water and a volumetric flask (9.7 % of the sample undissolved). Non-magnetic fraction (0.5 g) was exposed to a concentrated HF/HCl mixture in an open acid digestion and consequently treated with HNO<sub>3</sub> (Vander Auwera et al. 1998). 22.2 % of the sample remained undissolved.

The determination was carried out on the Spectr AA - 240 FS instrument (Varian) with the evaluation program in the PROMPT mode (maximum sample measurement time 10 s). Standards were prepared from certified calibration solutions Astasol (Analytika, s.r.o.). Fe, Na, and K were determined in the air-acetylene flame, other elements in the nitrous oxide-

acetylene flame. To suppress ionization in the case of Na, K, and Ca, cesium chloride solution was added to give a final concentration of 1000 mg/L of cesium in all solutions including the blank. Correction for non-specific absorption was performed. The measurement was done with a maximum error of  $\pm 3\%$ .

## **2.2. Calculation of the trajectory**

For calculation of the Porangaba bolide trajectory, only a low-quality security camera video of the bolide and two photographs of the atmospheric smoke trail visible after the bolide event were available. Detailed description of the calculations together with in-depth results is provided in Supplementary Data to the paper. The bolide event security camera video was used to determine the angular velocity of the body. Due to the high field distortion in combination with the event position in the upper right corner of the camera field, determining the beginning and end points of the track with sufficient accuracy was not possible.

### 3. Results

#### 3.1. Petrography and mineral composition

The Porangaba meteorite has been found shortly after the observed fall, and its very fresh nature is reflected in the absence of widespread weathering with the exception of weak veins on the surface of the fusion crust. These observed weathering features indicate a weathering grade of W0, according to the Wlotzka classification (Wlotzka, 1993). The structure of the specimen was significantly brecciated and rock fragments, including chondrules, were only slightly cemented. The relatively poor quality of the polished surface, the presence crumbling, relief etc., corresponds to a considerable sample incoherence. Furthermore, the specimen appears to be a heterogeneous mixture of fragments of different materials.

It was found that the main component of the sample is represented by fragments of enstatitic and rarely even forsteritic particles and isolated chondrules with a high proportion of forsteritic olivine in the matrix. The meteorite shows clearly visible and sharply defined chondrules and a fine-grained matrix (Figure 3).

Chondrule sizes vary from approximately 0.4 mm to 5 mm and they have a very complicated and unstable internal structure. The chondrules consist mainly of olivine (Fa<sub>21-25</sub>) mean Fa<sub>23.6</sub>, with percent mean deviation (PMD) - FeO 2.9%, *n*=44; and low-Ca pyroxene (Fs<sub>17-23</sub>Wo<sub>0.7-1.2</sub>) mean Fs<sub>20.0</sub> Wo<sub>0.96</sub>, Fs PMD 5.5%, Wo PMD 11.3%, *n*=52. Alkali-bearing glasses exhibit a wide range of chemical compositions. Most of the secondary feldspar grains are <2 μm in size, but some are larger.

The matrix is probably composed mainly of plagioclases and small fragments or even crystals of pyroxene. Moreover, irregularly bounded grains formed by Fe-Ni metal alloy were found in the matrix, too. It is clearly two-component and consists of a remission of α-(Fe, Ni) i.e. kamacite (usually about Fe<sub>95</sub>Ni<sub>5</sub>) and γ-(Fe, Ni) i.e. taenite (around Fe<sub>0.6</sub>Ni<sub>0.3</sub>). It was also found usually round grains, consisting of troilite (Stoichiometric FeS). Troilite quite often merges with the metal component. Furthermore, chromium spinelide grains were found to be quite rare in the matrix. This is, when converted to the contents of end members, made up of about 75% chromite component. In addition, an admixture of hercynitine and magnesiochromite components (both up to about 10 mol%) was found in spinelide. Chromites also contain slightly increased proportions of TiO<sub>2</sub> around 2% (approx. 2.5 mol% of ulvospinel component).

Recrystallization of the fine-grained matrix is visible in the thin section (Figure 3).

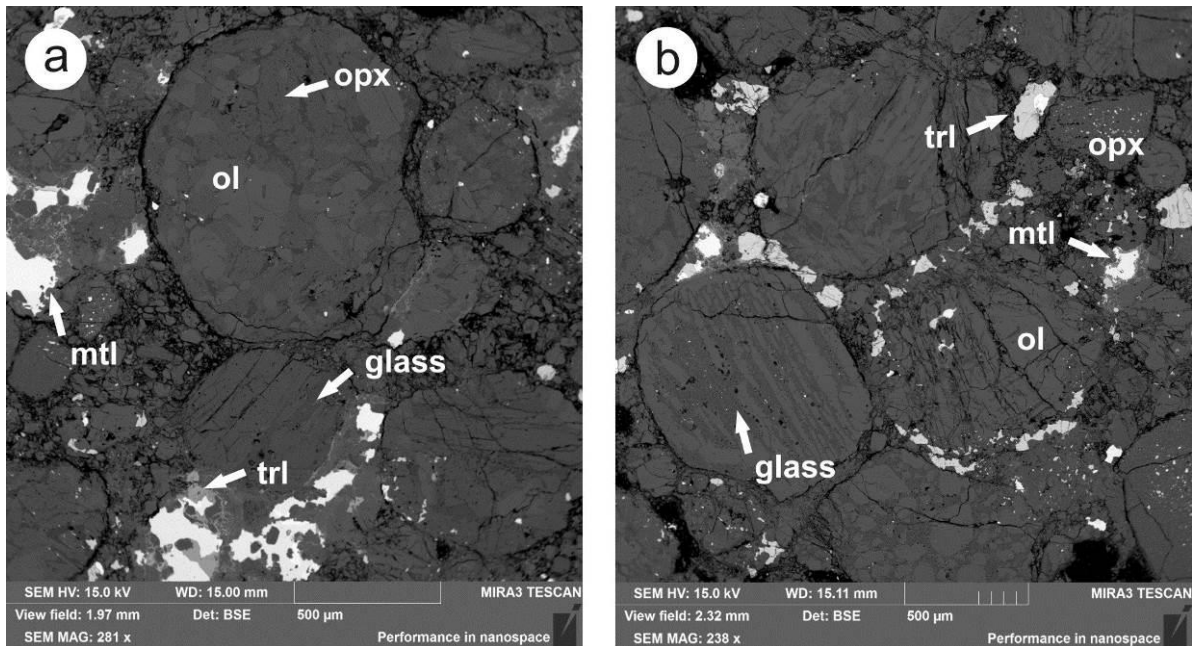


**Figure 3.** Backscattered electron images representing the texture of the Porangaba L4 ordinary chondrite include sharply defined chondrules and fine-grained matrices. Minerals: ol-olivine, opx-orthopyroxene, mtl-metals (kamacite-taenite), trl-troilite, and glass-glass.

Remission of plagioclase and Mg-Fe silicate components (enstatite) in chondrules and matrix, was frequently observed. While enstatite forms idiomorphic to hypidiomorphic crystals, the feldspar mass (alumosilicate Na-Ca) is clearly non-crystalline and contains many unidentifiable inclusions of submicrometric sizes.

Our investigations based on SEM and EDS/WDS measurements of average olivine and average low-Ca pyroxene composition show that these two minerals have composition of  $Fa_{23.6}$  and  $Fs_{20.0}Wo_{0.96}$ , respectively. This implies that the Porangaba meteorite should be classified as an ordinary chondrite L (Figure 4).

The absence of visible plagioclase grains suggest that the Porangaba meteorite is a petrologic type 4. Orthopyroxene (Fe enstatite) produces hypidiomorphic to xenomorphic grains and is found in both breccia and some chondrules. In addition to orthopyroxene, the sample also contains clinopyroxene diopside composition. This produces isolated crystals in the feldspar mass matrix of the sample and occasionally increases in the orthopyroxene grains.

Olivine and pyroxene in this L4 lithology show weak shock features, represented by the undulate extinction of olivine and orthopyroxene grains and the presence of irregular fractures corresponding to the shock stage S2, i.e., very weak impact shock metamorphism (5 -10 GPa) (Stöffler et al., 1991). The EBSD method did not confirm the presence of plagioclase-maskelynite conversion typical for higher shock stages.

Detailed composition of olivine and low-Ca pyroxene in comparison to several previous published L4 chondrites is shown in Table 1.a and Table 1.b.

The mineral modes obtained by the AZtec Phase Map Analysis were recalculated into % weight and are presented in Table S7. The distributions of the mineral phases and textures of the studied meteorite are shown in Figure 5.

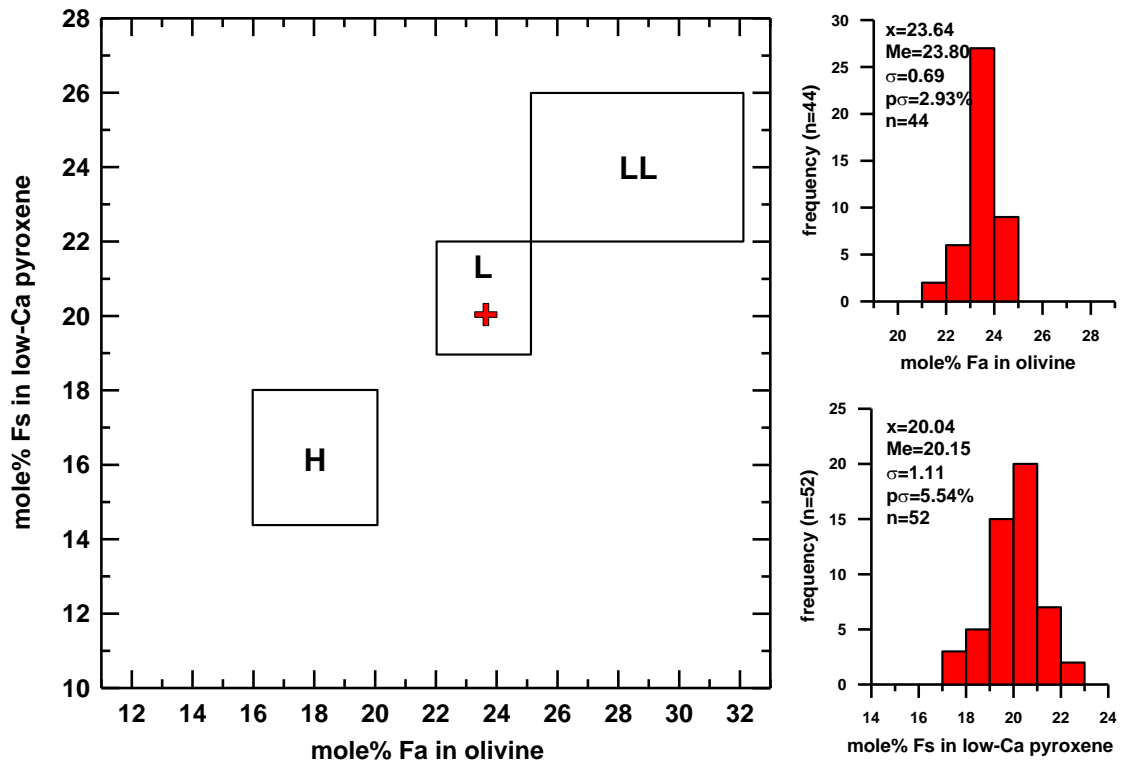


**Figure 4.** Classification scheme of the L4 Porangaba ordinary chondrite based on the molar olivine (fayalitic content) and low-Ca pyroxene (ferrosilite content) composition. H, L, and LL indicate typical ranges for H, L, and LL ordinary chondrites compiled from (Brearley and Jones, 1998). Fa-fayalite, Fs-ferrosilite,  $\bar{x}$ -average composition, Me-median,  $\sigma$ -mean deviation,  $p\sigma$ -percent mean deviation, and n-number of point analysis are also shown.

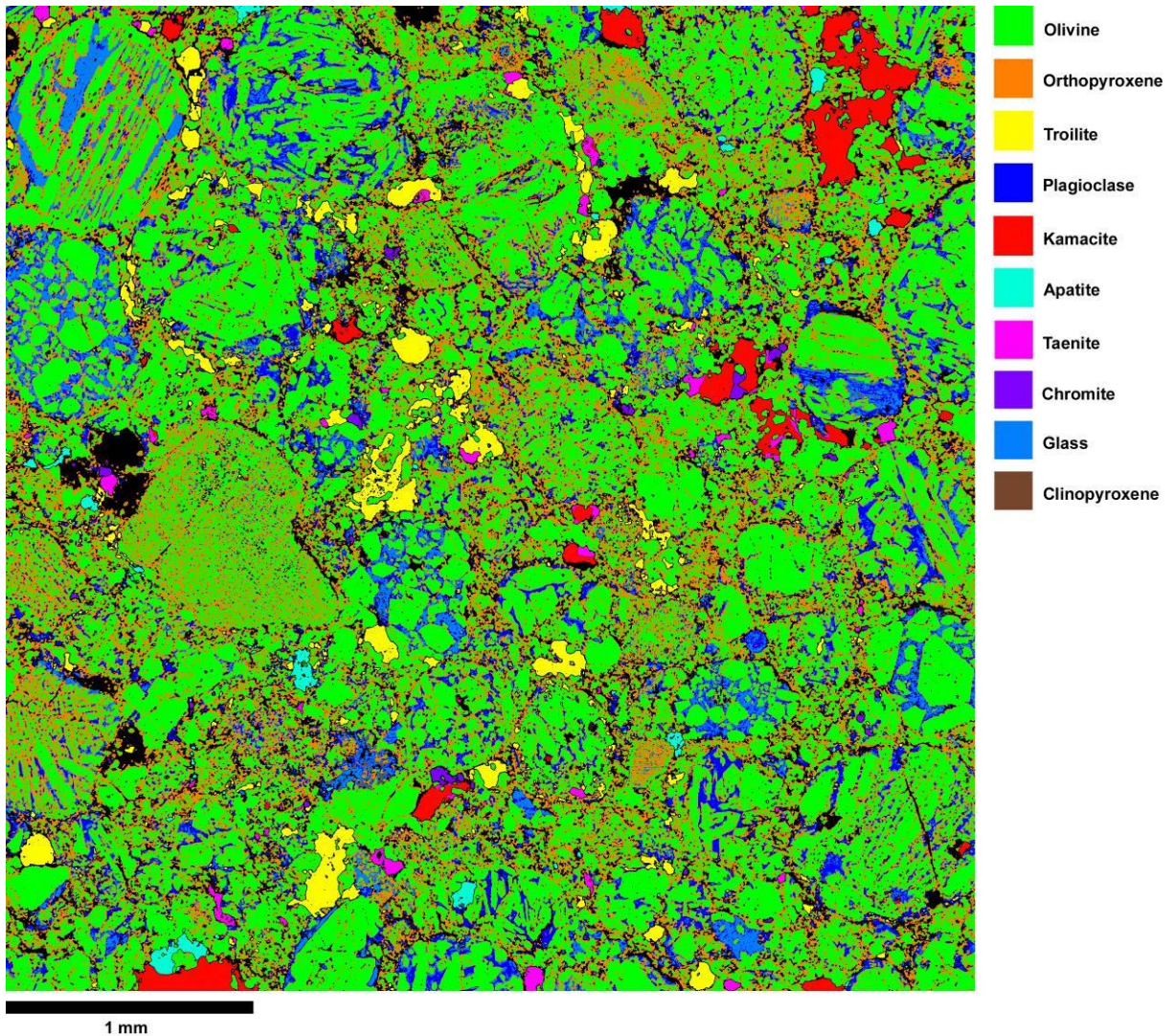


**Figure 5.** Phase distribution map of part of the studied thick section of the L4 Porangaba ordinary chondrite showing the distribution of the main rock-forming minerals and meteorite textures. The modal abundances of the minerals are as follows: olivine 43.8 wt %, orthopyroxene 25.6 wt %, clinopyroxene 2.8 wt %, plagioclase 4.5 wt %, kamacite 5.9 wt %, taenite 2.2 wt %, troilite 7.5 wt %, chromite 0.3 wt %, apatite 0.6 wt %, glass 6.5 wt %, and other minerals 0.3 wt %.

**Table 1.a.** Average electron microprobe analyses of olivine for Porangaba (this study) and a group of selected L4 meteorites (Dunn et al., 2010).

<b>Average electron microprobe analyses of olivine</b>					
<b>L4 Ordinary chondrites</b>	<b>Porangaba</b>	<b>Atarra</b>	<b>Bald Mountain</b>	<b>Rio Negro</b>	<b>Rupota</b>
SiO <sub>2</sub>	<b>38.33</b>	38.2	38.2	38.3	38.1
Cr <sub>2</sub> O <sub>3</sub>	<b>0.00</b>	0.11	0.09	0.03	<0.03
FeO	<b>21.89</b>	21.4	21.3	22.5	22.4
MnO	<b>0.47</b>	0.46	0.46	0.46	0.46
MgO	<b>39.31</b>	39.7	40.1	38.9	38.8
CaO	<b>0.00</b>	0.03	<0.03	0.04	0.05
Total	<b>100</b>	99.9	100.1	100.3	99.9
Cations based on 4 oxygens					
Si	<b>1.00</b>	0.99	0.99	1.00	1.00
Cr	<b>0.00</b>	0.00	0.00	0.00	0.00
Fe	<b>0.48</b>	0.46	0.46	0.49	0.49
Mn	<b>0.01</b>	0.01	0.01	0.01	0.01
Mg	<b>1.52</b>	1.54	1.55	1.51	1.51
Ca	<b>0.00</b>	0.00	0.00	0.00	0.00
Total	<b>3.1</b>	3.1	3.1	3.00	3.00
Fe/Mn	<b>48.0</b>	46.2	46.2	46.2	48.9
Fe/Mg	<b>0.32</b>	0.30	0.30	0.30	0.32
Fa	<b>23.6</b>	23.2	22.9	24.5	24.5

**Table 1.b.** Average electron microprobe analyses of low-Ca pyroxene for Porangaba (this study) and a group of selected L4 meteorites (Dunn et al., 2010).

<b>Average electron microprobe analyses of low-Ca pyroxene</b>					
<b>L4 Ordinary chondrites</b>	<b>Porangaba</b>	<b>Atarra</b>	<b>Bald Mountain</b>	<b>Rio Negro</b>	<b>Rupota</b>
SiO <sub>2</sub>	<b>55.32</b>	55.6	55.5	55.4	55.4
TiO <sub>2</sub>	<b>0.08</b>	0.14	0.13	0.15	0.18
Al <sub>2</sub> O <sub>3</sub>	<b>0.06</b>	0.16	0.18	0.36	0.23
Cr <sub>2</sub> O <sub>3</sub>	<b>0.20</b>	0.15	0.19	0.40	0.21
FeO	<b>13.7</b>	13.2	13.0	13.4	13.4
MnO	<b>0.48</b>	0.45	0.49	0.46	0.46
MgO	<b>29.51</b>	29.9	29.8	29.4	29.0
CaO	<b>0.64</b>	0.41	0.80	0.7	1.02
Na <sub>2</sub> O	<b>0</b>	0.03	<0.03	0.05	0.03
<b>Total</b>	<b>99.99</b>	100.0	100.1	100.2	99.9
<b>Cations based on 6 oxygens</b>					
Si	<b>1.98</b>	1.98	1.98	1.98	1.98
Ti	<b>0.00</b>	0.00	0.00	0.00	0.00
Al	<b>0.00</b>	0.01	0.01	0.02	0.01
Cr	<b>0.01</b>	0.00	0.01	0.01	0.01
Fe	<b>0.41</b>	0.39	0.39	0.40	0.40
Mn	<b>0.01</b>	0.01	0.01	0.01	0.01
Mg	<b>1.57</b>	1.59	1.59	1.56	1.55
Ca	<b>0.02</b>	0.02	0.03	0.03	0.04
Na	<b>0.00</b>	0.00	0.00	0.00	0.00
<b>Total</b>	<b>4.01</b>	4.01	4.01	4.01	4.01
Fe/Mn	<b>27.3</b>	28.9	26.3	29.2	29.2
Fe/Mg	<b>0.26</b>	0.25	0.24	0.26	0.26
Fs	<b>20.0</b>	20.2	19.9	20.6	20.7
Wo	<b>0.96</b>	0.8	1.5	1.3	2.0

Both Table 1.a. and Table 1.b. show very reasonable agreement between the mineralogy of the Porangaba and other meteorites classified as type L4. Particular very small deviations from other specimens presented in these tables can be found for cases of rare metal oxides such as  $\text{TiO}_2$  and  $\text{Al}_2\text{O}_3$ . On the other hand, the analysis of olivine exhibits a very good agreement with the typical composition of L4 representatives shown in the table. However, as shown in the following chapter, the bulk composition of Porangaba represents an interesting case of a meteorite exhibiting Fe/Mg ratios between those of L and H type of ordinary chondrites.

### 3.2. Bulk elemental composition

The bulk elemental composition of the Porangaba meteorite was first determined by SEM and EDS/WDS (MA) analysis. However, the studied meteorite surface exhibits significant heterogeneity (see Figure 5), so another four analytical techniques were used for comparative determination of the bulk elemental composition. They were CF-LIBS, LA-ICP-MS, ICP-MS and AAS. Comparison of the results obtained by each method mentioned above is summarized in Table 2.

**Table 2.** Comparison of ratios of selected chemical elements and magnesium analysed by various methods.

Weight ratio of elements [wt%/wt%]	L type ordinary chondrites [wt %] (Drouard et al., 2018)	Elemental analysis ICP-MS [wt %]	Elemental analysis AAS [wt %]	Minerals analyzed (MA) [wt %]	Elemental analysis CF-LIBS [wt %]	Elemental analysis LA-ICP-MS [wt %]
<b>Fe/Mg</b>	<b>1.44</b>	<b>1.936</b>	<b>1.705</b>	<b>1.682</b>	<b>1.942</b>	<b>1.337</b>
Si/Mg	1.24	-	-	1.235	0.620	1.989
Al/Mg	0.08	0.007	0.082	0.111	0.127	0.149
Ca/Mg	0.09	0.012	0.062	0.061	0.172	0.176
Na/Mg	0.05	0.016	0.066	0.069	0.018	0.120
Cr/Mg	0.03	0.001	0.002	0.021	0.042	0.029
Ni/Mg	0.08	0.146	0.291	0.050	0.043	0.107
Co/Mg	0.004	0.005	0.031	0.009	-	0.005
Ti/Mg		0.002	0.000	0.004	0.052	0.005

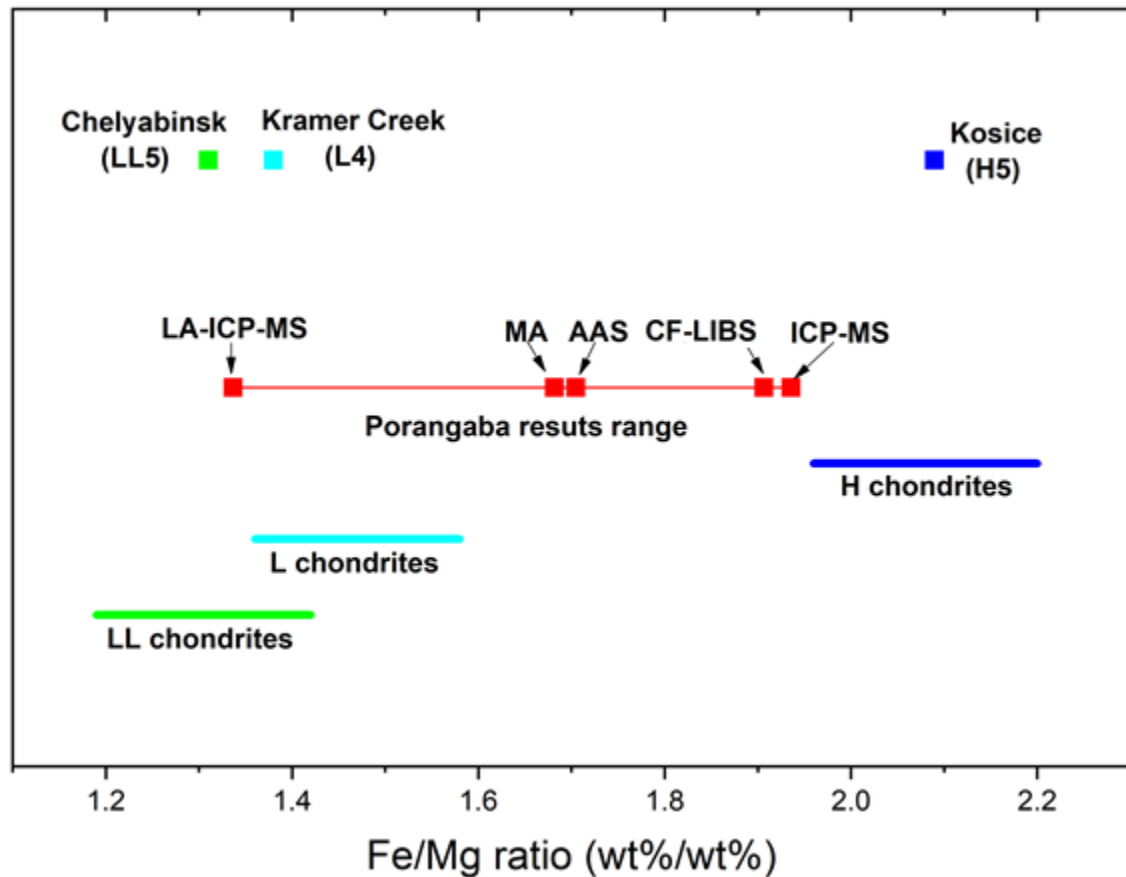


**Figure 6.** Comparison of the Fe/Mg ratio values of each H, L and LL (Nittler et al., 2004) ordinary chondrite chemical group together with results of each analysis (LA-ICP-MS, MA, CF-LIBS, AAS and ICP-MS). The results range from 1.337 (LA-ICP-MS) to 1.936 (ICP-MS). For reference, values of the Fe/Mg ratio of another three meteorites: Kosice (H5) (Ozdin et al., 2015), Kramer Creek (L4) (Gibson et al., 1977) and Chelyabinsk (LL5) (Galimov et al., 2013) are depicted.

The classification of the Porangaba meteorite specimen into the relevant chemical group was based on the value of the Fe/Mg ratio, which was previously published for a wide range of meteorites (Nittler et al., 2004). The authors of this study state that ordinary chondrites exhibit a trend of decreasing magnesium content with an increasing iron content in the order LL→L→H→EH. The range of the Fe/Mg values typical for LL, L and H chondrites together with the Porangaba value are depicted in Figure 6. The Porangaba specimen exhibits Fe/Mg ratio ranging from 1.936 (estimated by ICP-MS) to 1.337 (estimated by LA-ICP-MS). It is clearly visible that all the results are not in good agreement with values typical for L-chondrites. We believe that it is because of large heterogeneity of the specimen.

### 3.3. Trajectory and probable origin of the meteoroid

The Porangaba sporadic bolide was a very slow meteor; its geocentric velocity before entering the Earth's gravitational field was  $12.6 \pm 2.1$  km/s (without the effect of deceleration) with the geocentric radiant RA =  $316.5 \pm 7.5^\circ$  (right ascension), DEC =  $10.6 \pm 1.4^\circ$  (declination). Due to the methodology of orbit computation, the deceleration was not involved in the calculations. Large uncertainties exist in the heliocentric orbital elements, as do uncertainties of the geocentric radiant position and geocentric velocity, which are caused by the input data presented in this work (*Tables 1-3*).

In order to calculate the atmospheric path of the bolide and orbit of the meteoroid in the Solar System, photographs of the trail from Lençóis Paulista and Tatuí were used. The calculated values are shown in the Table 3 and the details are provided in the Section S1 of the Supplementary Data to the paper. The projection of the beginning of the visible atmospheric path, depicted schematically in Figure 7, was located at the coordinates S23.009° W48.186° near the village of Pirambóia, São Paulo, Brazil. The height of the bolide at this time was  $49.7 \pm 4.2$  kilometres above the Earth's surface. The end of the projection of the visible atmospheric path was located at S23.163° W48.157°, which is near the city of Porangaba. The height of the bolide at this time was  $19.0 \pm 1.8$  km above the Earth's surface. The absolute magnitude of the Porangaba bolide was not calculated and neither was an estimate of the body's initial mass before entering the Earth's atmosphere. In any case, the body entered the Earth's atmosphere at a high zenith angle of  $60.5^\circ$  and its terminal height was very low (less than 20 km above the Earth's surface).

The estimated projection of the derived Porangaba orbits in the Solar System is depicted in Figure 8. It shows that the Porangaba initial body probably comes from the outer side of the Main asteroid belt.

**Table 3.** Heliocentric orbital elements (J2000.0) of Porangaba, calculated using the software UFOOrbit (SonotaCo, 2009)

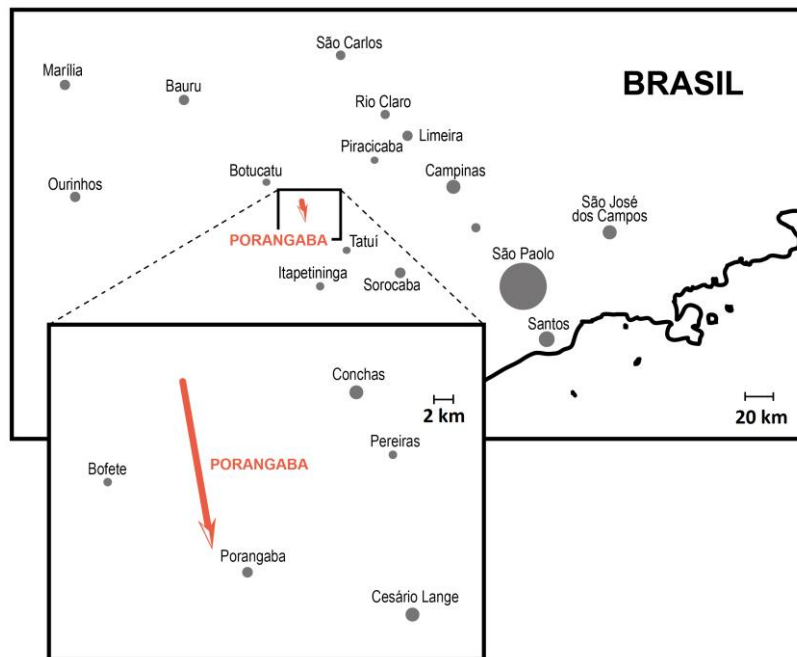
Semimajor axis	$A$	$2.54 \pm 1.10$ AU
Eccentricity	$E$	$0.64 \pm 0.11$
Perihelion distance	$Q$	$0.91 \pm 0.05$ AU
Aphelion distance	$Q$	$4.17 \pm 2.20$ AU
Argument of perihelion	$\omega$	$142.8 \pm 6.7^\circ$
Longitude of ascending node	$\Omega$	$288.921 \pm 0.001^\circ$
Inclination	$I$	$8.6 \pm 3.2^\circ$
Orbital period	$P$	$4.04 \pm 2.91$ y
Heliocentric velocity	$v_h$	$38.1 \pm 1.4$ km/s

**Table 4.** Geocentric radiant, geocentric velocity of Porangaba, calculated using the software (SonotaCo, 2009)

Geocentric velocity	$v_g$	$12.6 \pm 2.1$ km/s
Radiant right ascension	$RA$	$316.5 \pm 7.5$ °
Radiant declination	$DEC$	$10.6 \pm 1.4$ °

**Table 5.** The atmospheric path parameters of Porangaba calculated using the software UFOOrbit (SonotaCo, 2009)

Beginning latitude of the atmospheric path projection	$LAT_B$	$-23.009 \pm 0,021$ °
Beginning longitude of the atmospheric path projection	$LON_B$	$-48.186 \pm 0.029$ °
Beginning height of the atmospheric path projection	$H_B$	$49.7 \pm 4.2$ km
Terminal latitude of the atmospheric path projection	$LAT_E$	$-23.163 \pm 0.013$ °
Terminal longitude of the atmospheric path projection	$LON_E$	$-48.157 \pm 0.024$ °
Terminal height of the atmospheric path projection	$H_E$	$19.0 \pm 1.8$ km

**Figure 7.** Projection of the Porangaba atmospheric path over the Earth's surface

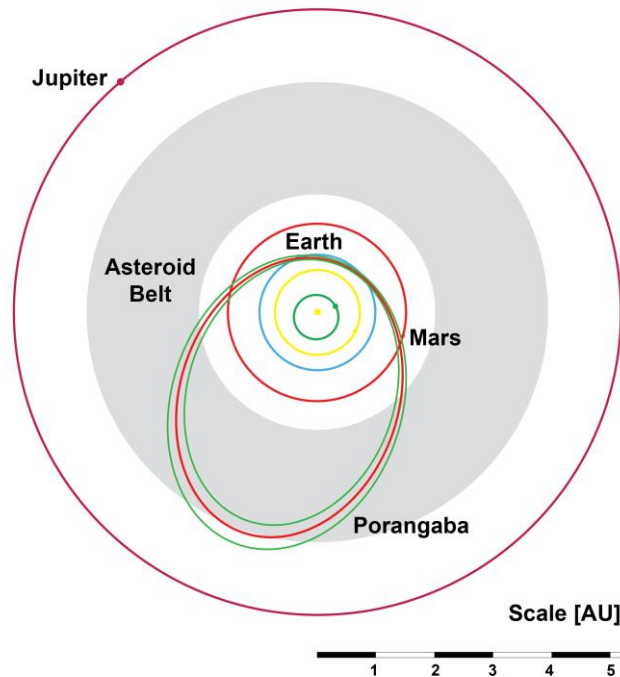


**Figure 8.** Projection of the derived Porangaba orbits in the Solar System. The mean orbit is shown in red, while the green orbits represent those based on combinations of the Porangaba orbital element errors. The latter appear in the following order (from the smallest semi-major axis, in the parenthesis number of the solution):  $q-e-$  (6),  $e-$  (4),  $q+e-$  (8),  $q-$  (2), mean orbit (1),  $q+$  (3). The boundaries of the main asteroid belt are depicted - inner, middle and outer (marked in gray), defined by asteroid orbits with average eccentricity in a given part of the main-belt.

### 3.4. Simulation of Porangaba meteor spectra

In addition to the laboratory CF-LIBS analytical technique, emission spectroscopy can also contribute to the analysis of the chemical composition of meteors (Berezhnoy and Borovicka, 2010; Borovicka et al., 1999; Borovička and Betlem, 1997; Jenniskens, 2007; Madiedo et al., 2013). In our previous study, we published a Calibration Free analysis of Perseid and Leonid meteors (Ferus et al., 2018). Porangaba was not recorded on a spectrographic camera. However, regarding the future potential of meteor spectroscopy, the application of Calibration Free calculations and the experimental approaches employing laser ablation for meteor spectra simulation, we briefly discuss in this section the simulated meteor spectra of this interesting specimen.

If a body disintegrates and none of its fragments are found as meteorites, the spectrum becomes the only record of its chemical composition. In such case, spectroscopic techniques play an important role. However, the current state of art in this field is not optimistic. There are only two cases of parallel record of both meteor spectra and an existence of a sample of the corresponding meteorite: Žďár nad Sázavou (9 December 2014) and Neuschwanstein (4 April, 2002) (Ferus, 2015). Comparisons of their spectroscopic analyses together with

reference measurements using LIBS and other laboratory methods have not been published for either meteor.

In the case of Porangaba, we calculated synthetic spectra based on the concentrations obtained from the elemental analysis. These are shown in Figure 9, panels A and B. The synthetic spectra were generated by summing the Voigt spectral line profiles with the emission intensities calculated from the available spectroscopic data from the National Institute of Standards and Technology (NIST) website database (A. Kramida et al., 2019). The ratio of the neutral atoms to ions (singly- and doubly-charged ions were included) was calculated using an iterative method of Saha's equations solution (Zaghloul, 2004). The code used for the simulation includes also a simple radiative transfer model (a homogeneous plasma block of changeable size) which is able to partially correct the emission intensities for the self-absorption.

We calculated two types of the synthetic spectra. The first (Figure 9, panel B) is the simulation of the laboratory ablation experiment. In this case the input parameters were set according to the experimental ones. The plasma temperature was set to 8258 K, according to the temperature estimated using the Saha-Boltzmann plot in Figure S11 of the Supplementary Data section. The plasma pressure was set to 1 atmosphere. For the radiative transfer model a block of plasma 3 mm on each side was used. The two spectra in panel B were computed from the same data and with the same parameters. They differ only by the chosen instrumental function. One of them has a low resolution (corresponding to the meteor spectrographic camera resolution) and the other has a higher resolution, corresponding to the high-resolution spectra obtained in laboratory measurements by the Echelle spectrograph.

The second type of the synthetic spectra (Figure 9, panel A) simulates the radiation which would be emitted during the impact of the studied body into the atmosphere. The real observed spectra of meteor plasma contain two components corresponding to two different temperatures, usually around 5000 K and 10 000 K (Borovicka, 1993). For this reason, we have calculated three synthetic spectra using different temperatures: 5000 K is used for the “cold” part of the meteor plasma and 10 000 K and 12 000 K are used for the second “hot” component. It is assumed that this component comes from a very hot area near the front of the meteor and its temperature varies. To simulate the conditions in the meteoric plasma we set the plasma pressure and the size of the radiative transfer model block to 100 Pa and 1 m respectively. The resulting three-component synthetic spectrum is shown in Figure 9, panel A.

Finally, panel C shows two experimental emission spectra of Porangaba from the ablation point C1.

As can be seen in the Figure 9, the synthetic spectra (panel B) and the ablation spectrum of Porangaba (panel C) is in reasonable agreement. However, in some narrow spectral regions (e.g., near 422.5 nm) small differences between theoretical simulation and experimental data can be noticed. They are caused mainly by the self-absorption effect in the nonhomogeneous ablation plasma which can't be simulated by the used radiative transfer model for homogeneous environments. Another effect which make classical quantitative interpretation inaccurate is the matrix effect. However, the presented technique of calibration free calculation reduces these effects by careful selection of the spectral lines used for the analysis and is able to calculate the elemental ratios from real observed spectra with sufficient precision.

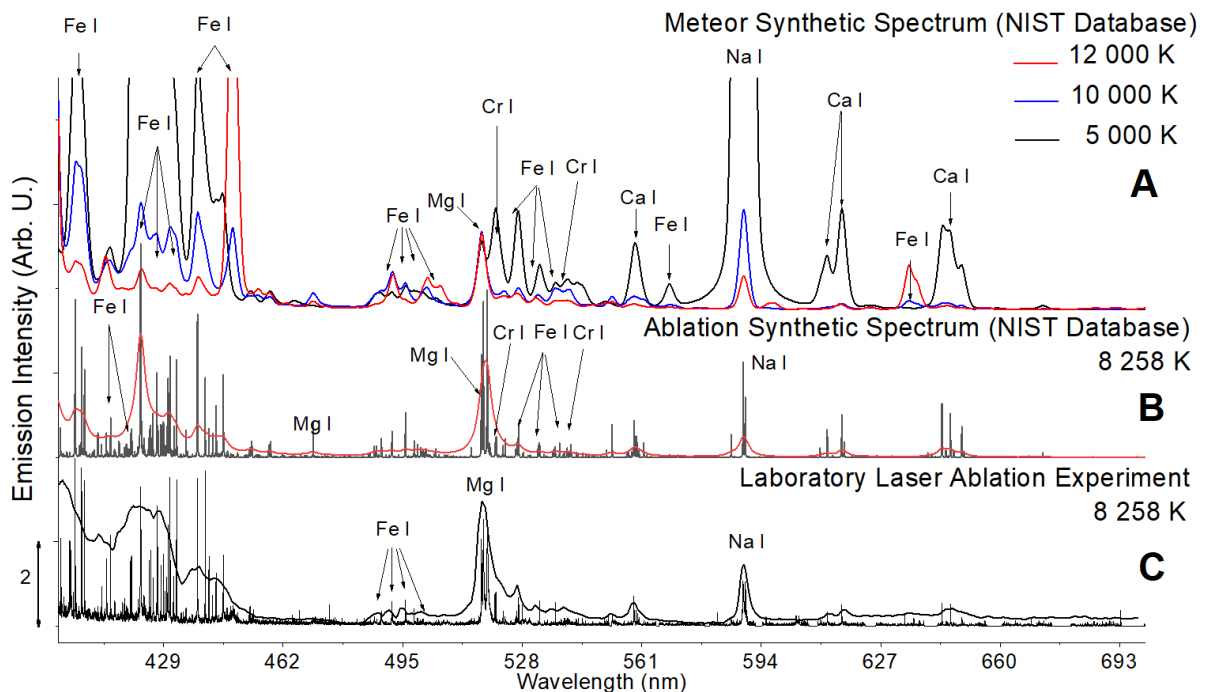


**Figure 9.** Panel A shows a simulation of the Porangaba meteor spectra calculated using three temperature components (12 000 K, 10 000 K and 5 000 K) and NIST Database (A. Kramida et al., 2019). Panel B shows a simulation of the Porangaba ablation spectra (B, calculated using one temperature component, 8 258 K. This temperature was determined from the LIBS analysis using the Saha-Boltzmann plane plot). The spectra were calculated in both high- and low- resolutions. Panel C shows experimental laboratory data recorded using a high-resolution spectrograph and a low-resolution spectral camera (the same as the camera used for real meteor spectra observation).

## 4. Discussion

The Porangaba meteorite specimen represents a fresh L4 type chondrite material originating from a small meteoroid with an expected diameter of tens of centimetres (Collins et al., 2005). The undulatory extinction of olivine and orthopyroxene grains and the presence of irregular fractures in the part A of our specimen (Figure 2; Panel A1-A2) (estimated by SEM, EDS/WDS and EBSD) correspond to its very weak shock stage S2 (Stöffler et al., 1991). This fact implies that the Porangaba parent body must have been exposed to shock pressure 5 – 10 GPa and has undergone a post-shock temperature increase from 20 – 50 °C. The lack of significant weathering also signifies that the material mostly retains its original composition in interplanetary space.

The heterogeneous brecciated structure of the meteorite, as described above, could imply that the Porangaba meteorite originates from body with a rubble-pile structure, where the parent body was probably collisionally disrupted and gravitationally reassembled together with another different geochemical and petrological types of meteoroids. For example, the composition of the Morávka (Borovicka et al., 2003) meteorite was determined as a mixture of H5 and H6 ordinary chondrites. Yet another example is the Itokawa asteroid, which was examined by Hayabusa spacecraft in December 2005 and which is considered a rubble-pile structured body, too (Abe et al., 2006).

The bulk elemental composition results of each analysis (depicted in Table 2) are quite different to each other and none of them quite fit to the L chondrite group. Especially in the case of the Fe/Mg ratio, which was chosen for the classification of the meteorite specimen to an appropriate geochemical group, there is a significant variance, which makes it difficult to classify the meteorite specimen into one group correctly. The Fe/Mg results of individual analyses are 1.37 (LA-ICP-MS), 1.682 (MA), 1.806 (CF-LIBS), 1.707 (AAS) and 1.936 (ICP-MS). The typical range of Fe/Mg for L chondrite group is 1.38 – 1.52 (Nittler et al., 2004). The graphic demonstration of ranges of Fe/Mg ratios for LL, L and H chemical group together with the average value of the Porangaba meteorite and other three meteorites are depicted in Figure 6. It is clearly visible that none of these results agree with the L group. The MA, CF-LIBS, AAS and ICP-MS results lie between the values for L and H groups. In the case of LA-ICP-MS value of Fe/Mg even corresponds to the LL group. On the other hand, it is clearly visible that the Fe/Mg ratio of Chelyabinsk LL5 meteorite (Galimov et al., 2013), Kramer Creek L4 meteorite (Gibson et al., 1977) and Košice meteorite H5 (Ozdin et al., 2015)

perfectly fit to their respective groups. However, the content of fayalite in olivine ( $\text{Fa}_{23.6}$ ) and the content of ferrosilite ( $\text{Fs}_{17-23}$ ) and wolastonite ( $\text{Wo}_{0.96}$ ) in low-Ca pyroxene (obtained by SEM EDS/WDS, Figure 4.) show that Porangaba meteorite specimen perfectly corresponds to the L group (Brearley and Jones, 1998). Nevertheless, classification based on the analysis of olivine and low-Ca pyroxene takes into consideration only the composition of these two minerals, but not the others, such as the abundance of Fe-Ni metal grains, which, according to the results of previously published analysis accessible on (Mindat.org, 2016) and the Meteoritical Bulletin Database (Grossman, 2015) state that Fe-Ni grains occupy ~6 % of the area of the Porangaba meteorite. We note that except SEM EDS/WDS, all the methods are destructive (although ablation techniques evaporate a very small amount of the sample) and therefore the sample has been further divided in several pieces analysed by techniques mentioned above.

Considering the very limited accuracy of calculations based on the very poor-quality data, we provide only tentative orbital parameters and list of several bodies (Table S2 in Supplementary Information section) with close orbital elements. Nevertheless, given the short list of meteorites with documented elemental compositions, mineralogies and sources in the Solar System, we still believe that even such raw data can be valuable, because the knowledge of the distribution of different types of asteroids in the Solar system according to their chemical composition could give us important information about the formation and evolution of our Solar system. This distribution has been studied for many years and it is still not exactly clear. Some studies (DeMeo and Carry, 2013; Gradie and Tedesco., 1982) have shown the existence of a global compositional heliocentric gradient in the asteroid main belt. For example, S-type asteroids dominate in the inner part and C-types in the outer part of the main asteroid belt. Furthermore, the oxidation level of bodies generally increases with the heliocentric distance i.e. oxidised asteroids have typically larger heliocentric distances than reduced asteroids.

Careful analysis and retrograde calculation of the mean orbital elements of the potential Porangaba parent body are described in detail in the Supplementary Data (Section S1, particularly S1.3.). On the basis of this analysis, we can conclude that the body exhibits a resonance with Jupiter orbital trajectory in a ratio 3:1 and 4:1. These resonances are in good agreement with the Kirkwood gaps (See Table S3 and (Minton and Malhotra, 2009)).

The calculations are introduced in detail in the Chapter S1.1. The estimated orbital trajectory is depicted in Figure 8. In this computation, the heliocentric distance of Porangaba was determined to be  $2.54 \pm 1.10$  AU. Based on the Tisserand's parameter of the meteor orbit ( $T_j =$

3.414), we assume that the parent body of the Porangaba meteorite is probably an unknown object from the main asteroid belt. A summary of potential parent bodies of the Porangaba meteorite is given in the Supplementary Data (Table S2). One of the probable parent bodies is asteroid 1998 SU27, classified as a transient Sq type. The spectrum of this object has already been measured. However, we should note that the accuracy of this determination is strictly limited by the very scarce knowledge of the meteor descent parameters. In general, based on the facts above, we can state that it is a body exhibiting orbital resonance 3:1 with respect to Jupiter and it belongs to the group Q or O based on the SMASSII taxonomy.

Orbital trajectories in these resonances are generally unstable in longer time horizons and the perihelion is moving from the orbits outside the trajectory of the Earth to the inner part of the Solar System. Such movement also means that the bodies reach a collisional course with Earth. The perihelion is moved to the space between Earth and Sun and the aphelion can be usually found in the main asteroid belt. In the current literature we can find that by a comparison of the reflectance spectra, albedo and colour characteristics using the SMASSII taxonomy (Bus and Binzel, 2002) with types of bodies in the main asteroid belt, ordinary chondrites type L and LL, such as Porangaba, are very close to Q-type of asteroids.

## 5. Conclusions

The Porangaba meteorite specimen represents a fresh chondritic material with a very heterogeneous brecciated character. The specimen appears to be a heterogeneous mixture of fragments of different materials.

Based on the molar olivine ( $\text{Fa}_{23.6}$ ) and low-Ca pyroxene ( $\text{Fs}_{17-23}$ ,  $\text{Wo}_{0.96}$ ) composition obtained by SEM EDS/WDS, the Porangaba can be classified as an L chondrite. However, the Fe/Mg ratio obtained by five independent techniques, shows something different. In the case of MA, CF-LIBS, AAS and ICP-MS analysis, the Fe/Mg ratio lies in between values typical for L and H chondrites. In the case of LA-ICP-MS analysis, the meteorite specimen even appears to be an LL chondrite. This wide range of Fe/Mg ratio is probably due to variations of FeNi metal in studied specimen. Based on these results and based on the specimen very heterogeneous structure, we believe that the Porangaba meteorite probably originates from a body with rubble-pile structure.

Our calculations (however based on very rough data from several photos and security cameras) indicate that the parent body of Porangaba meteoroid is an unknown object on the outer edge of the main asteroid belt exhibiting orbital resonance 3:1 with respect to the Jupiter.

We also provide a laboratory simulation of meteor spectra emissions that can be used for at least qualitative comparison with spectra from sporadic meteors with similar composition to the Porangaba (L4 Ordinary Chondrite) recorded by high-speed video-cameras equipped with simple grating spectrographs.

Despite the unsatisfactory number of meteorites with known major properties and orbits in the Solar system, in comparison to the total number of observed falls, we believe that with constantly improving observing techniques, the number of these information-rich meteorites will increase rapidly over time and that the Porangaba meteorite is now becoming one of them. Ultimately, the greater the number of these meteorites will be, step by step, the amazing story of the Solar system will become more and more uncovered.

## Acknowledgements

The research has been supported by the programme of Regional Cooperation between the Regions and the Institutes of the Czech Academy of Sciences in 2017 (projects no.:

R200401721 and R200401521), in 2018 and 2019 (projects no.: R200401721 and R200401801) and ERDF/ESF "Centre of Advanced Applied Sciences" (No. CZ.02.1.01/0.0/0.0/16\_019/0000778). Support of the Czech Science Foundation within the project reg. no. 18-27653S is acknowledged.

## References

- A.~Kramida, Yu.~Ralchenko, J.~Reader, 2019. NIST Atomic Spectra Database (ver. 5.7).
- Abe, S., Mukai, T., Hirata, N., Barnouin-jha, O.S., Cheng, A.F., Demura, H., Gaskell, R.W., Hashimoto, T., Hiraoka, K., Honda, T., Kubota, T., Matsuoka, M., Mizuno, T., 2006. Mass and Local Topography Measurements of Itokawa by Hayabusa 75, 1344–1347.
- Afanasiev, V.L., Kalenichenko, V. V., Karachentsev, I.D., 2007. Detection of an intergalactic meteor particle with the 6-m telescope. <https://doi.org/10.1134/s1990341307040013>
- Berezhnoy, A.A., Borovicka, J., 2010. Formation of molecules in bright meteors. *Icarus* 210, 150–157. <https://doi.org/10.1016/j.icarus.2010.06.036>
- Borovicka, J., 1993. A fireball spectrum analysis. *Astron. Astrophys.* 279, 627–645.
- Borovička, J., Betlem, H., 1997. Spectral analysis of two Perseid meteors. *Planet. Space Sci.* 45, 563–575. [https://doi.org/10.1016/S0032-0633\(97\)00024-X](https://doi.org/10.1016/S0032-0633(97)00024-X)
- Borovička, J., Spurný, P., Brown, P., Wiegert, P., Kalenda, P., Clark, D., Shrubený, L., 2013. The trajectory, structure and origin of the Chelyabinsk asteroidal impactor. *Nature* 503, 235–237.
- Borovicka, J., Spurny, P., Kalenda, P., Tagliaferri, E., 2003. The Moravka meteorite fall: 1. Description of the events and determination of the fireball trajectory and orbit from video records. *Meteorit. Planet. Sci.* 38, 975–987. <https://doi.org/10.1111/j.1945-5100.2003.tb00293.x>
- Borovicka, J., Stork, R., Bocek, J., 1999. First results from video spectroscopy of 1998 Leonid meteors. *Meteorit. {&} Planet. Sci.* 34, 987–994.
- Brearley, A.J., Jones, R.H., 1998. Chondritic meteorites. *Planet. Mater.* 3.
- Brown, P., Ceplecha, Z., Hawkes, R.L., Wetherill, G., Beech, M., Mossman, K., 1994. The orbit and atmospheric trajectory of the Peekskill meteorite from video records. *Nature* 367, 624–626. <https://doi.org/10.1038/367624a0>
- Brown, P., Pack, D., Edwards, W.N., ReVelle, D.O., Yoo, B.B., Spalding, R.E., Tagliaferri, E., 2004. The orbit, atmospheric dynamics, and initial mass of the Park Forest meteorite. *Meteorit. Planet. Sci.* 39, 1781–1796. <https://doi.org/10.1111/j.1945-5100.2004.tb00075.x>
- Bus, S.J., Binzel, R.P., 2002. Phase II of the small main-belt asteroid spectroscopic survey: A feature-based taxonomy. *Icarus* 158, 146–177.
- Ceplecha, Z., 1961. Multiple fall of Příbram meteorites photographed. 1. Double-station photographs of the fireball and their relations to the found meteorites. *Bull. Astron. Institutes Czechoslov.* 12, 21.
- Ciucci, A., Corsi, M., Palleschi, V., Rastelli, S., Salvetti, A., Tognoni, E., 1999. New Procedure for Quantitative Elemental Analysis by Laser-Induced Plasma Spectroscopy. *Appl. Spectrosc.* 53, 960–964. <https://doi.org/10.1366/0003702991947612>

- Collins, G.S., Melosh, H.J., Marcus, R.A., 2005. Earth Impact Effects Program: A Web-based computer program for calculating the regional environmental consequences of a meteoroid impact on Earth. *Meteorit. Planet. Sci.* 40, 817–840. <https://doi.org/10.1111/j.1945-5100.2005.tb00157.x>
- Cousin, A., Sautter, V., Fabre, C., Maurice, S., Wiens, R.C., 2012. Textural and modal analyses of picritic basalts with ChemCam Laser-Induced Breakdown Spectroscopy. *J. Geophys. Res.* 117. <https://doi.org/10.1029/2012JE004132>
- De Giacomo, A., 2011. A novel approach to elemental analysis by Laser Induced Breakdown Spectroscopy based on direct correlation between the electron impact excitation cross section and the optical emission intensity. *Spectrochim. ACTA PART B-ATOMIC Spectrosc.* 66, 661–670. <https://doi.org/10.1016/j.sab.2011.09.003>
- Dell'Aglio, M., De Giacomo, A., Gaudiuso, R., De Pascale, O., Longo, S., 2014. Laser Induced Breakdown Spectroscopy of meteorites as a probe of the early solar system. *Spectrochim. ACTA PART B-ATOMIC Spectrosc.* 101, 68–75. <https://doi.org/10.1016/j.sab.2014.07.011>
- Dell'Aglio, M., De Giacomo, A., Gaudiuso, R., De Pascale, O., Senesi, G.S., Longo, S., 2010. Laser Induced Breakdown Spectroscopy applications to meteorites: Chemical analysis and composition profiles. *Geochim. Cosmochim. Acta* 74, 7329–7339. <https://doi.org/10.1016/j.gca.2010.09.018>
- DeMeo, F.E., Carry, B., 2013. The Taxonomic Distribution of Asteroids from Multi-filter All-sky Photometric Surveys. *Icarus* 226, 723–741. <https://doi.org/10.1016/j.icarus.2013.06.027>
- Drouard, A., Vernazza, P., Loehle, S., Gattacceca, J., Vaubaillon, J., Zanda, B., Birlan, M., Bouley, S., Colas, F., Eberhart, M., Hermann, T., Jorda, L., Marmo, C., Meindl, A., Oefele, R., Zamkotsian, F., Zander, F., 2018. Probing the use of spectroscopy to determine the meteoritic analogues of meteors. <https://doi.org/10.1051/0004-6361/201732225>
- Dunn, T.L., McSween, H.Y., McCoy, T.J., Cressey, G., 2010. Analysis of ordinary chondrites using powder X-ray diffraction: 2. Applications to ordinary chondrite parent-body processes. *Meteorit. Planet. Sci.* 45, 139–160. <https://doi.org/10.1111/j.1945-5100.2009.01012.x>
- Ferus, M., 2015. , private communication with Ing. Lenža and Dr. Borovička.
- Ferus, M., Koukal, J., Lenža, L., Srba, J., Kubelik, P., Laitl, V., Zanozina, E.M., Vana, P., Kaiserova, T., Knizek, A., Civiš, S., 2017. Recording and evaluation of high resolution optical meteor spectra and comparative laboratory measurements using laser ablation of solid meteorite specimens, in: *International Conference on Transparent Optical Networks*. <https://doi.org/10.1109/ICTON.2017.8024864>
- Ferus, M., Koukal, J., Lenža, L., Srba, J., Kubelík, P., Laitl, V., Zanozina, E.M., Vána, P., Kaiserová, T., Knížek, A., Rimmer, P., Chatzitheodoridis, E., Civiš, S., 2018. Calibration-free quantitative elemental analysis of meteor plasma using reference laser-induced breakdown spectroscopy of meteorite samples. *Astron. Astrophys.* 610. <https://doi.org/10.1051/0004-6361/201629950>
- Galimov, E., Kolotov, V.P., Nazarov, M.A., Kostitsyn, Y.A., 2013. Analytical results for the material of the Chelyabinsk meteorite. <https://doi.org/10.1134/S0016702913070100>
- Gibson, E.K., Lange, D.E., Keil, K., 1977. The Kramer Creek, Colorado meteorite: a new L4

chondrite 12.

- Gounelle, M., Spurny, P., Bland, P.A., 2006. The orbit and atmospheric trajectory of the Orgueil meteorite from historical records. *Meteorit. Planet. Sci.* 41, 135–150.  
<https://doi.org/10.1111/j.1945-5100.2006.tb00198.x>
- Gradie, J., Tedesco, E., 1982. Compositional structure of the asteroid belt. *Science* (80-. ). 216, 1405–1407.
- Gritsevich, M.I., 2008. The Pribram, Lost City, Innisfree, and Neuschwanstein falls: An analysis of the atmospheric trajectories. *Sol. Syst. Res.* 42, 372–390.  
<https://doi.org/10.1134/S003809460805002X>
- Grossman, J., 2015. Porangaba. *Meteorit. Bull. Database*.
- Haramura, H., Kushiro, I., Yanai, K., 1983. Chemical composition of Antarctic meteorites. *Mem. Natl. Inst. Polar Res.* 30, 109–121.
- Hornackova, M., Plavcan, J., Rakovsky, J., Porubcan, V., Ozdin, D., Veis, P., 2014. Calibration-free laser induced breakdown spectroscopy as an alternative method for found meteorite fragments analysis. *Eur. Phys. JOURNAL-APPLIED Phys.* 66.  
<https://doi.org/10.1051/epjap/2014130465>
- Hornáčková, M., Plavčan, J., Rakovský, J., Porubčan, V., Ozdín, D., Veis, P., 2014. Calibration-free laser induced breakdown spectroscopy as an alternative method for found meteorite fragments analysis. *Eur. Phys. J. Appl. Phys.* 66, 10702.  
<https://doi.org/10.1051/epjap/2014130465>
- Jenniskens, P., 2007. Quantitative meteor spectroscopy: Elemental abundances. *Adv. Sp. Res.* 39, 491–512. <https://doi.org/10.1016/j.asr.2007.03.040>
- Koukal, J., Srba, J., Gorková, S., Lenža, L., Ferus, M., Civiš, S., Knížek, A., Kubelík, P., Kaiserová, T., Váňa, P., 2016. Meteors and meteorites spectra. *Proc. IMC* 1–6.
- Lasue, J., Wiens, R.C., Clegg, S.M., Vaniman, D.T., Joy, K.H., Humphries, S., Mezzacappa, A., Melikechi, N., McInroy, R.E., Bender, S., 2012. Remote laser-induced breakdown spectroscopy (LIBS) for lunar exploration. *J. Geophys. Res.* 117.  
<https://doi.org/10.1029/2011JE003898>
- List of meteorites with a complete “lineage” [WWW Document], 2019. . Seznam meteoritů s rodokmenem Wikipedie - otevřená Encykl.
- Madiedo, J.M., Trigo-Rodriguez, J.M., Konovalova, N., Williams, I.P., Castro-Tirado, A.J., Ortiz, J.L., Cabrera-Cano, J., 2013. The 2011 October Draconids outburst - II. Meteoroid chemical abundances from fireball spectroscopy. *Mon. Not. R. Astron. Soc.* 433, 571–580. <https://doi.org/10.1093/mnras/stt748>
- McCrosky, R.E., Posen, A., Schwartz, G., Shao, C.Y., 1971. Lost City meteorite - Its recovery and a comparison with other fireballs. *J. Geophys. Res.* 76, 4090-.  
<https://doi.org/10.1029/JB076i017p04090>
- Mindat.org, 2016. Porangaba meteorite, Porangaba, São Paulo, Brazil [WWW Document].
- Minton, D.A., Malhotra, R., 2009. A record of planet migration in the main asteroid belt. *Nature* 457, 1109–1111. <https://doi.org/10.1038/nature07778>
- Nittler, L.R., McCoy, T.J., Clark, P.E., Murphy, M.E., Trobka, J.I., Jarosewich, E., 2004. Bulk element compositions of meteorites: a guide for interpreting remote-sensing geochemical measurements of planets and asteroids. *Antarct. Meteor. Res.* 233–253.

- Ozdin, D., Plavcan, J., Hornackova, M., Uher, P., Porubcan, V., Veis, P., Rakovsky, J., Toth, J., Konecny, P., Svoren, J., 2015. Mineralogy, petrography, geochemistry, and classification of the Kosice meteorite. *Meteorit. & Planet. Sci.* 50, 864–879. <https://doi.org/10.1111/maps.12405>
- Senesi, G.S., 2014. Laser-Induced Breakdown Spectroscopy (LIBS) applied to terrestrial and extraterrestrial analogue geomaterials with emphasis to minerals and rocks. *EARTH-SCIENCE Rev.* 139, 231–267. <https://doi.org/10.1016/j.earscirev.2014.09.008>
- Siraj, A., Loeb, A., 2019. Discovery of a Meteor of Interstellar Origin.
- SonotaCo, A., 2009. Meteor shower catalog based on video observations in 2007–2008. *WGN J. Int. Meteor Organ* 37, 55–62.
- Stöffler, D., Keil, K., Scot, E.R.D., 1991. Shock metamorphism of ordinary chondrites 55.
- Thompson, J.R., Wiens, R.C., Barefield, J.E., Vaniman, D.T., Newsom, H.E., Clegg, S.M., 2006. Remote laser-induced breakdown spectroscopy analyses of Dar al Gani 476 and Zagami Martian meteorites. *J. Geophys. Res.* 111. <https://doi.org/10.1029/2005JE002578>
- Tognoni, E., Cristoforetti, G., Legnaioli, S., Palleschi, V., 2010. Review Calibration Free Laser- Induced Breakdown Spectroscopy: State of the art. *Spectrochim. Acta Part B At. Spectrosc.* 65, 1–14.
- Van Der Auwera, J., Bologne, G., Roelandts, I., Duchesne, J.C., 1998. Inductively coupled plasma-mass spectrometric (ICP-MS) analysis of silicate rocks and minerals. *Geol. Belgica* 1, 49–53.
- Welten, K.C., Caffee, M.W., Hillemonds, D.J., Coy, T.J.M., Masarik, J., 2011. Cosmogenic radionuclides in L5 and LL5 chondrites from Queen Alexandra Range , Antarctica : Identification of a large L/LL5 chondrite shower with a preatmospheric mass of approximately 50 , 000 kg 198, 177–198. <https://doi.org/10.1111/j.1945-5100.2010.01142.x>
- Wlotzka, F., 1993. A Weathering Scale for the Ordinary Chondrites. *Meteoritics* 28, 460–460.
- Zaghloul, M.R., 2004. Reduced formulation and efficient algorithm for the determination of equilibrium composition and partition functions of ideal and nonideal complex plasma mixtures. *Phys. Rev. E* 69, 26702. <https://doi.org/10.1103/PhysRevE.69.026702>

## Supporting Information

### Author Contributions

*SC, MF, LL, JK, JH invented the research*

*MF, SC, JK, JS, AK, LP, AP and LL wrote the paper*

*MF, AK, PK, PV, LP and SC performed ablation experiments*

*JH performed EBSD and SEM analysis*

*MF, LP, LL and SC evaluated the data*

*JK calculated orbital parameters*

*DM and MB mineralogical analysis and consultation*

*BD performed the AAS*

*PK and VL calculated the synthetic spectra*

*RNP, MWD, GG, CAdP and RdOS found and provided the meteorite and performed preliminary analyses*

*TV performed the LA-ICP-MS*

### Highlights

- Complete study of Porangaba meteorite using a wide range of techniques.
- Calculations of Porangaba orbital parameters.
- Porangaba becomes one of rare examples of meteorites with complete lineage.
- Porangaba was identified as relatively iron rich L4 type.